

Vacuum Stability Constraints on the Enhancement of the $h \rightarrow \gamma\gamma$ Rate in the MSSM

Teppei Kitahara[†]

*Department of Physics, The University of Tokyo,
Tokyo 113-0033, Japan*

Abstract

The ATLAS and CMS collaborations discovered a new boson particle. If the new boson is the Higgs boson, the diphoton signal strength is 1.5 - 1.8 times larger than the Standard Model (SM) prediction, while the WW and ZZ signal strengths are in agreement with the SM one. In the Minimal Supersymmetric Standard Model (MSSM), overall consistency can be achieved by a light stau and the large left-right mixing of staus. However, a light stau and large left-right mixing of staus may suffer from vacuum instability. We first apply the vacuum meta-stability condition to the Higgs to diphoton decay rate in the MSSM. We show that the vacuum meta-stability severely constrains the enhancement to the Higgs to diphoton rate. For example, when the lighter stau mass is 100 GeV, the upper bound on the enhancement to the Higgs to diphoton rate becomes 25%.

KEYWORDS: Supersymmetry, Higgs boson, Higgs to diphoton rate

[†] Electronic address: kitahara@hep-th.phys.s.u-tokyo.ac.jp

1 Introduction

The ATLAS [1] and CMS [2] collaborations at the Large Hadron Collider (LHC) have announced the discovery of the new boson particle around the mass region of 126 GeV in the search for the Standard Model (SM) Higgs boson with significances of 6σ (ATLAS) and 5σ (CMS), respectively. This boson has a signal strength almost consistent with the prediction of SM Higgs boson except in the diphoton channel. The signal strength $\mu(X)$ is defined by

$$\begin{aligned}\mu(X) &\equiv \frac{\sigma(pp \rightarrow h)BR(h \rightarrow X)}{\sigma(pp \rightarrow h)_{SM}BR(h \rightarrow X)_{SM}} \\ &= \frac{\sigma(pp \rightarrow h)}{\sigma(pp \rightarrow h)_{SM}} \times \frac{\Gamma(h \rightarrow \text{All})_{SM}}{\Gamma(h \rightarrow \text{All})} \times \frac{\Gamma(h \rightarrow X)}{\Gamma(h \rightarrow X)_{SM}},\end{aligned}\quad (1)$$

where X indicates a final state of the Higgs decay, for example $b\bar{b}$, WW or $\gamma\gamma$. Both the ATLAS and the CMS collaborations have reported that the observed diphoton signal strength is 1.5 – 1.8 times larger than the SM prediction value [1, 2],

$$\begin{aligned}\mu(\gamma\gamma)_{\text{ATLAS}} &= 1.8 \pm 0.5, \\ \mu(\gamma\gamma)_{\text{CMS}} &= 1.56 \pm 0.43.\end{aligned}\quad (2)$$

On the other hand, $\mu(ZZ)$ and $\mu(WW)$ are consistent with the SM,

$$\begin{aligned}\mu(ZZ^{(*)} \rightarrow 4l)_{\text{ATLAS}} &= 1.4 \pm 0.6, \\ \mu(ZZ^{(*)} \rightarrow 4l)_{\text{CMS}} &= 0.7_{-0.3}^{+0.4}, \\ \mu(WW^{(*)} \rightarrow l\nu l\nu)_{\text{ATLAS}} &= 1.3 \pm 0.5, \\ \mu(WW^{(*)} \rightarrow l\nu l\nu)_{\text{CMS}} &= 0.6 \pm 0.4.\end{aligned}\quad (3)$$

Although statistics of accumulated events are still low, this enhanced diphoton signal strength implies various new physics models beyond the SM [3, 4, 5, 6, 7, 8, 9, 10, 11, 12, 13, 14, 15, 16, 17, 18]. The Minimal Supersymmetric (SUSY) Standard Model (MSSM) scenarios are known to be able to enhance $\mu(\gamma\gamma)$ in the decoupling limit, where the lighter CP-even Higgs h can acquire the mass of 126 GeV [19, 20, 21, 22], and in the non-decoupling limit, where the heavier CP-even Higgs H has the mass of 126 GeV [23, 24, 25]. In the former scenario, a light stau and the large left-right mixing of staus can appropriately enhance $\mu(\gamma\gamma)$ [19, 20, 21, 22]. However, it was pointed out that the light stau and the large left-right mixing of staus may suffer from vacuum instability [26, 27, 28]. For this reason, in this paper we analyze the Higgs to diphoton rate in a broad parameter region in the MSSM, applying vacuum stability conditions. We do not assume any particular high energy supersymmetry breaking structure. In addition, we show that vacuum stability severely constrains the enhancement to the Higgs to diphoton rate, and that there is an upper bound of 25% on the enhancement to the Higgs to diphoton rate when the lighter stau mass is larger than 100 GeV.

This paper is organized as follows. In section 2, the enhancement to the diphoton signal strength $\mu(\gamma\gamma)$ in the MSSM will be reviewed, and the necessity for light stau and large left-right mixing of staus will be discussed. In section 3, we will discuss the

vacuum meta-stability of staus. In section 4, we will analyze numerically the Higgs to diphoton rate under the stau vacuum meta-stability condition in a broad parameter region. Section 5 is devoted to our conclusions and discussion.

2 Corrections to the signal strength from the MSSM sector

In this section, let us briefly review the enhancement to the diphoton signal strength $\mu(\gamma\gamma)$ in the MSSM.

In general, Eq. (1) implies that there are three ways to enhance the diphoton signal strength $\mu(\gamma\gamma)$. The first way is to enhance the Higgs production cross-section $\sigma(pp \rightarrow h)$. Since the Higgs production cross-section is dominated by gluon fusion $\sigma(gg \rightarrow h)$, this can be achieved by simply adding new colored particles [29, 22]. The second way is to suppress the Higgs total decay width $\Gamma(h \rightarrow \text{All})$. Since the Higgs mainly decays into $b\bar{b}$, one should suppress the Higgs to $b\bar{b}$ partial width $\Gamma(h \rightarrow b\bar{b})$. For example, in the MSSM, large squark left-right mixing parameters, a small CP-odd Higgs mass (M_A), and a moderate value of $\tan\beta$ ($\langle H_d^0 \rangle = v_1 = v \cos\beta$, $\langle H_u^0 \rangle = v_2 = v \sin\beta$, $\tan\beta = v_2/v_1$ and $v \simeq 174$ GeV) can lead to the desired suppression of the Higgs to $b\bar{b}$ partial width, so-called “small α_{eff} scenario” [30]. Singlet multiplets extended MSSM (e.g. NMSSM) can also lead to suppress the Higgs to $b\bar{b}$ partial width because of singlet-doublet Higgs mixing effects [31]. The last way is to enhance the Higgs to $\gamma\gamma$ partial width $\Gamma(h \rightarrow \gamma\gamma)$ itself. However, since these three ways are intricately related, the analysis of enhancement to the diphoton signal strength is involved.

In the MSSM, if one takes the observations Eqs. (2) and (3) into account, the situation becomes somewhat simplified. Eq. (1) also implies that the first two ways are independent of the Higgs decay channel (X), and only the third pattern depends on the Higgs decay channel. In addition, in the MSSM, the Higgs to WW and ZZ partial widths are almost equal to the SM values, since only gauge couplings contribute at leading order and SUSY particle contributions receive loop suppression. Therefore, if one employs the first or second way to enhance the diphoton signal strength, additional enhancement to the WW and ZZ signal strengths are inevitable. However, in fact, the observed signal strengths except for diphoton, particularly for WW and ZZ are in good agreement with the SM prediction in the range of 1σ [1, 2]. Hence, in the following, we assume that $\sigma(pp \rightarrow h)/\sigma(pp \rightarrow h)_{SM} \times \Gamma(h \rightarrow \text{All})_{SM}/\Gamma(h \rightarrow \text{All})$ is almost unity, and we consider only the third way. For that reason, we have investigated not the diphoton signal strength $\mu(\gamma\gamma)$ but the Higgs to diphoton partial width as compared with the SM prediction $\Gamma(h \rightarrow \gamma\gamma)/\Gamma(h \rightarrow \gamma\gamma)_{SM}$ in detail in this paper.

In the MSSM, the Higgs to diphoton partial width arises dominantly from the W boson loop, and sub-dominantly from the top quark loop. An analytic expression for the Higgs to diphoton partial width is given in Refs. [32, 33] and it is rewritten as follows,

$$\Gamma(h \rightarrow \gamma\gamma) = \frac{\alpha^2 m_h^3}{1024\pi^3} \left| \frac{g_{hWW}}{m_W^2} A_1^h(\tau_W) + \sum_f \frac{2g_{hff}}{m_f} N_{c,f} Q_f^2 A_{\frac{1}{2}}^h(\tau_f) + A_{SUSY}^{h\gamma\gamma} \right|^2, \quad (4)$$

where $\tau_i = m_h^2/4m_i^2$, m_h is the lightest CP-even Higgs mass, $N_{c,i}$ is the number of colors of particle i , Q_i is electric charge of particle i , and

$$A_{\text{SUSY}}^{h\gamma\gamma} = \sum_{\tilde{f}} \frac{g_{h\tilde{f}\tilde{f}}}{m_{\tilde{f}}^2} N_{c,\tilde{f}} Q_{\tilde{f}}^2 A_0^h(\tau_{\tilde{f}}) + \sum_{i=1,2} \frac{2g_{hx_i^+x_i^-}}{m_{x_i^\pm}} A_{\frac{1}{2}}^h(\tau_{x_i^\pm}) + \frac{g_{hH^+H^-}}{m_{H^\pm}^2} A_0^h(\tau_{H^\pm}), \quad (5)$$

with loop functions $A_i(\tau)^h$ the Higgs coupling constants g given in Appendix A.

At the heavy particle loop limit $\tau_i \ll 1$, the loop functions $A_i(\tau)^h$ take the following asymptotic value,

$$A_1^h \rightarrow 7, A_{\frac{1}{2}}^h \rightarrow -\frac{4}{3}, A_0^h \rightarrow -\frac{1}{3}. \quad (6)$$

Since the Higgs mass is 126 GeV and the top quark mass is 173.2 GeV [34], the loop functions of W and top quark loop are given by

$$A_1^h(\tau_W) = 8.36, 3 \times \left(\frac{2}{3}\right)^2 \times A_{\frac{1}{2}}^h = -1.84. \quad (7)$$

The Charged Higgs loop cannot sufficiently enhance the Higgs to diphoton rate since the Higgs coupling constant ($g_{hH^+H^-}$) is dominated by gauge couplings. The Chargino loop also cannot account for sufficient enhancement for the same reason and by $\tan\beta$ suppression [35]. On the other hand, since sfermions with large left-right mixing can have a large Higgs coupling constant ($g_{h\tilde{f}\tilde{f}}$), a light sfermion loop can sufficiently enhance the Higgs to diphoton rate. A light stop and sbottom loop, however, would not be appropriate to enhance the diphoton signal strength. These loops usually bring larger suppression of the gluon fusion rate than the enhancement of the Higgs to diphoton rate [29, 19]. This is the reason that the Higgs to diphoton amplitude is dominantly constructed by a W boson loop, but the hgg amplitude is dominantly constructed by a top quark loop. On the other hand, a stau loop does not influence the gluon fusion since stau does not carry color charge. Hence, in the MSSM, only a stau loop would be appropriate to enhance the diphoton signal strength.

The stau loop correction to the Higgs to diphoton amplitude is roughly proportional to $|m_\tau\mu\tan\beta|/m_{\tilde{\tau}_1}^2$ in the large $\mu\tan\beta$ region, where $m_{\tilde{\tau}_1}$ is the lighter stau mass. The corresponding Feynman diagram is shown in Figure 1. Light stau and large left-right mixing, i.e. large $\mu\tan\beta$, can sufficiently enhance the Higgs to diphoton rate, so-called ‘‘light stau scenario’’ [19, 21, 24, 22]. We obtain a simple formula for the leading stau corrections as follows,

$$\frac{\Gamma(h \rightarrow \gamma\gamma)}{\Gamma(h \rightarrow \gamma\gamma)_{SM}} \simeq \left(1 + \sum_{i=1,2} 0.05 \frac{m_\tau\mu\tan\beta}{m_{\tilde{\tau}_i}^2} x_L^{\tau_i} x_R^{\tau_i} \right)^2, \quad (8)$$

where stau mass eigenstates are given by $\tilde{\tau}_i = x_L^{\tau_i} \tilde{\tau}_L + x_R^{\tau_i} \tilde{\tau}_R$, $(x_L^{\tau_i})^2 + (x_R^{\tau_i})^2 = 1$.

Furthermore, the light stau scenario is also motivated by the anomalous magnetic moment of the muon [21, 36], where a 3.2σ discrepancy between the experimentally measured value a_μ^{exp} and the theoretical prediction value in the SM a_μ^{SM} , $\Delta a_\mu = a_\mu^{\text{exp}} -$

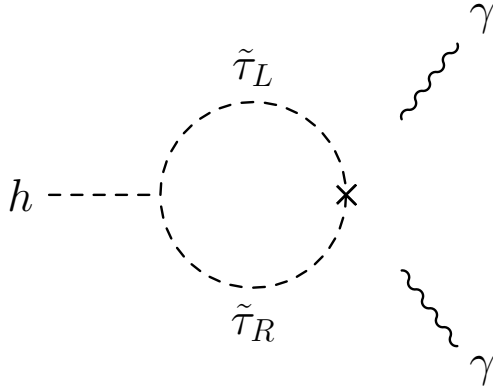


Figure 1: Feynman diagram which gives rise to an enhancement to the Higgs to diphoton rate in the mass insertion method. The cross represents the left-right mixing of staus.

$a_\mu^{\text{SM}} = (26.1 \pm 8.0) \times 10^{-10}$ [37] is observed. The reason for this is that light stau is compatible light μ -slepton when one considers high energy physics, and light μ -slepton and large $\tan \beta$ are favored to explain the discrepancy of the anomalous magnetic moment of the muon [38].

3 The Vacuum meta-stability constraints

In the MSSM, the large left-right mixing of staus can enhance the Higgs to diphoton rate as compared to the SM prediction. However, it is known that large left-right mixing and thus large $\mu \tan \beta$ may suffer from vacuum instability [26, 27]. The scalar potential develops the new charge-breaking minimum which leads to the $\tilde{L} \neq 0$ or $\tilde{\tau}_R \neq 0$ vacuum for sufficiently large $\mu \tan \beta$. And then, the minimum becomes lower than the ordinary electroweak-breaking minimum which leads to the $\tilde{L} = 0$ and $\tilde{\tau}_R = 0$ and $v \neq 0$ vacuum. In order to prohibit vacuum decay to charged-breaking vacuum, the lifetime of the electroweak-breaking vacuum is required to be longer than the age of the universe.

The vacuum transition rate from the false vacuum to the true vacuum can be evaluated by semiclassical technique [39]. Then, the imaginary part of the energy of the false vacuum determines the vacuum transition rate to the true vacuum. In the semiclassical technique, one evaluates the energy of the false vacuum state using the path integral method in Euclidean space-time. The vacuum transition rate per unit volume is evaluated as follows,

$$\frac{\Gamma}{V} = Ae^{-B}, \quad (9)$$

where a precise value of the coefficient A is difficult to evaluate. However, it does not depend dramatically on the parameters of the theory, and one can roughly estimate it at the fourth power of the typical scale in the potential,

$$A \simeq (100 \text{ GeV})^4. \quad (10)$$

In contrast, the power index B is a sensitive parameter of the vacuum transition rate per unit volume. It can be evaluated by an $O(4)$ symmetric solution as follows,

$$B = S_E[\bar{\phi}(\rho)] - S_E[\phi^f], \quad (11)$$

where ρ is a radial coordinate in four-dimensional spacetime, $S_E[\phi]$ is the Euclidean action as follows,

$$S_E[\phi(\rho)] = \int_0^\infty 2\pi^2 \rho^3 d\rho \left[\frac{1}{2} \left(\frac{d\phi}{d\rho} \right)^2 + V(\phi) \right], \quad (12)$$

ϕ^f is the value of the fields at false vacuum and $\bar{\phi}$ is the bounce configuration. The bounce configuration is a stationary point of the action and also satisfies the following boundary condition,

$$\lim_{\rho \rightarrow \infty} \bar{\phi}(\rho) = \phi^f, \quad \left. \frac{d\bar{\phi}(\rho)}{d\rho} \right|_{\rho=0} = 0. \quad (13)$$

On the other hand, the current value of the Hubble parameter given by $H_0 \simeq 1.5 \times 10^{-42}$ GeV. When the vacuum transition rate per unit volume Γ/V is smaller than the fourth power of H_0 , i.e. the lifetime of false vacuum is longer than the age of the universe, the power index B is larger than 403.6. Therefore, the vacuum meta-stability condition is approximately given as follows,

$$B \gtrsim 400. \quad (14)$$

A first study of the meta-stability condition of the stau sector has been conducted in Ref. [28], where the bounce configuration in three-field space (up-type neutral Higgs field and left- and right-handed stau field) was evaluated numerically. This study was done at tree level which only includes the dominant top/stop loop correction. The scalar potential, expanded around the electroweak-breaking vacuum in three-field space is given as follows,

$$\begin{aligned} V = & \frac{1}{2} m_Z^2 \sin^2 \beta (1 + \Delta_t) \phi^2 + (m_L^2 + \frac{g^2 - g'^2}{4} v_2^2) \tilde{L}^2 + (m_{\tilde{\tau}_R}^2 + \frac{g'^2}{2} v_2^2) \tilde{\tau}_R^2 \\ & - 2y_\tau \mu \tilde{L} \tilde{\tau}_R (v_2 + \frac{\phi}{\sqrt{2}}) + \frac{g^2 - g'^2}{2\sqrt{2}} v_2 \phi \tilde{L}^2 + \frac{g'^2}{\sqrt{2}} v_2 \phi \tilde{\tau}_R^2 + \frac{m_Z^2 \sin^2 \beta (1 + \Delta_t)}{2\sqrt{2} v_2} \phi^3 \\ & + \frac{m_Z^2 (1 + \Delta_t)}{16v^2} \phi^4 + \frac{g^2 + g'^2}{8} \tilde{L}^4 + \frac{g'^2}{2} \tilde{\tau}_R^2 + (y_\tau^2 - \frac{1}{2} g'^2) \tilde{L}^2 \tilde{\tau}_R^2 + \frac{g^2 - g'^2}{8} \phi^2 \tilde{L}^2 \\ & + \frac{g'^2}{4} \phi^2 \tilde{\tau}_R^2, \end{aligned} \quad (15)$$

where $H_u^0 = v_2 + \phi/\sqrt{2}$ and Δ_t is the leading log term of the one loop corrections for top/stop loops,

$$\Delta_t = \frac{3}{2\pi^2} \frac{y_t^4}{g^2 + g'^2} \log \frac{\sqrt{m_{\tilde{t}_1}^2 m_{\tilde{t}_2}^2}}{m_t^2}. \quad (16)$$

When the Higgs boson mass accomplishes 126 GeV, Δ_t has to be about 1. The scalar potential Eq. (15) includes only real parts of scalar bosons. Note that because the tau Yukawa coupling is $y_\tau = m_\tau/v_1$, the first term in the second line of Eq. (15) is proportional to $\mu \tan \beta$ for large $\tan \beta$. Therefore, this term can make a new minimum point of the scalar potential and thus has negative influence on vacuum stability.

The obtained approximate meta-stability conditional function [28] is as follows,

$$|\mu \tan \beta| < 76.9\sqrt{m_{\tilde{L}}m_{\tilde{\tau}_R}} + 38.7(m_{\tilde{L}} + m_{\tilde{\tau}_R}) - 1.04 \times 10^4 \text{ GeV}. \quad (17)$$

Note that the vacuum meta-stability condition is sensitive only to $m_{\tilde{L}}^2$, $m_{\tilde{\tau}_R}^2$ and $\mu \tan \beta$, but not $\tan \beta$ or μ itself, and neither Δ_t nor A_τ . In Ref. [28], it is assumed that the H_u^0 mass term, $\mu^2 + m_{H_u}^2$, is negative in order to get a vacuum expectation value v_2 . However, it is known that even when $\mu^2 + m_{H_u}^2$ is positive, correct electroweak symmetry breaking can be accomplished because when the H_d^0 component is integrated out, the H_u^0 mass term can become effectively negative [40]. Therefore, whether $\mu^2 + m_{H_u}^2$ is negative or not, the vacuum condition does not change. In order to check this, we analyzed the shape and the global minimum of the scalar potential and probed the upper bound of μ requiring that the electroweak-breaking minimum is the global minimum (see Appendix B). As a result, we found that regardless of the sign of $m_{H_u}^2$, the parameter $m_{H_u}^2$ does not affect the upper bound of μ .

We applied this vacuum meta-stability condition to the Higgs to diphoton rate. This condition means that large $\mu \tan \beta$ and small stau mass are severely restricted. As a result, the enhancement to the Higgs to diphoton rate by light stau loop is also severely restricted.

4 Numerical analysis

In this section, we analyze numerically the Higgs to diphoton partial width as compared with the SM prediction $\Gamma(h \rightarrow \gamma\gamma)/\Gamma(h \rightarrow \gamma\gamma)_{SM}$ and apply the stau vacuum meta-stability condition to the $\Gamma(h \rightarrow \gamma\gamma)/\Gamma(h \rightarrow \gamma\gamma)_{SM}$ in a broad parameter region.

The lower bound of the stau mass is obtained by various collider experiments [41],

$$m_{\tilde{\tau}_1} > 81.9 \text{ GeV}, \quad (18)$$

and we naively adopt the lower mass bound $m_{\tilde{\tau}_1} \geq 100 \text{ GeV}$ in the following calculation.

In Figure 2, the dependence of $\Gamma(h \rightarrow \gamma\gamma)/\Gamma(h \rightarrow \gamma\gamma)_{SM}$ in the $\mu - m_{\tilde{L}}$ plane for $m_{\tilde{\tau}_R} = m_{\tilde{L}}$ (left-hand side), as well as in the $m_{\tilde{L}} - m_{\tilde{\tau}_R}$ plane for $\mu = 600 \text{ GeV}$ (right-hand side) are shown. Solid lines represent contours of $\Gamma(h \rightarrow \gamma\gamma)/\Gamma(h \rightarrow \gamma\gamma)_{SM}$. Dashed lines represent contours of the lighter stau mass $m_{\tilde{\tau}_1}$. The gray (dark gray) areas are the regions where the lighter stau is tachyonic. The yellow (mostly white) areas are $m_{\tilde{\tau}_1} \geq 100 \text{ GeV}$. In addition, the red (gray) areas are the regions where the vacuum meta-stability condition (17) is broken. We considered fixed values of $\tan \beta = 20$ (top panel) and $\tan \beta = 60$ (bottom panel). In all panels, $M_A = 1 \text{ TeV}$, $M_3 = 1 \text{ TeV}$, $M_2 = 300 \text{ GeV}$, $A_\tau = 0 \text{ GeV}$, $m_{\tilde{Q}_3} = m_{\tilde{t}_R} = m_{\tilde{b}_R} = 850 \text{ GeV}$, other squark masses are 1 TeV and $A_t = 1.7 \text{ TeV}$, which gives $m_h \sim 126 \text{ GeV}$ at the two

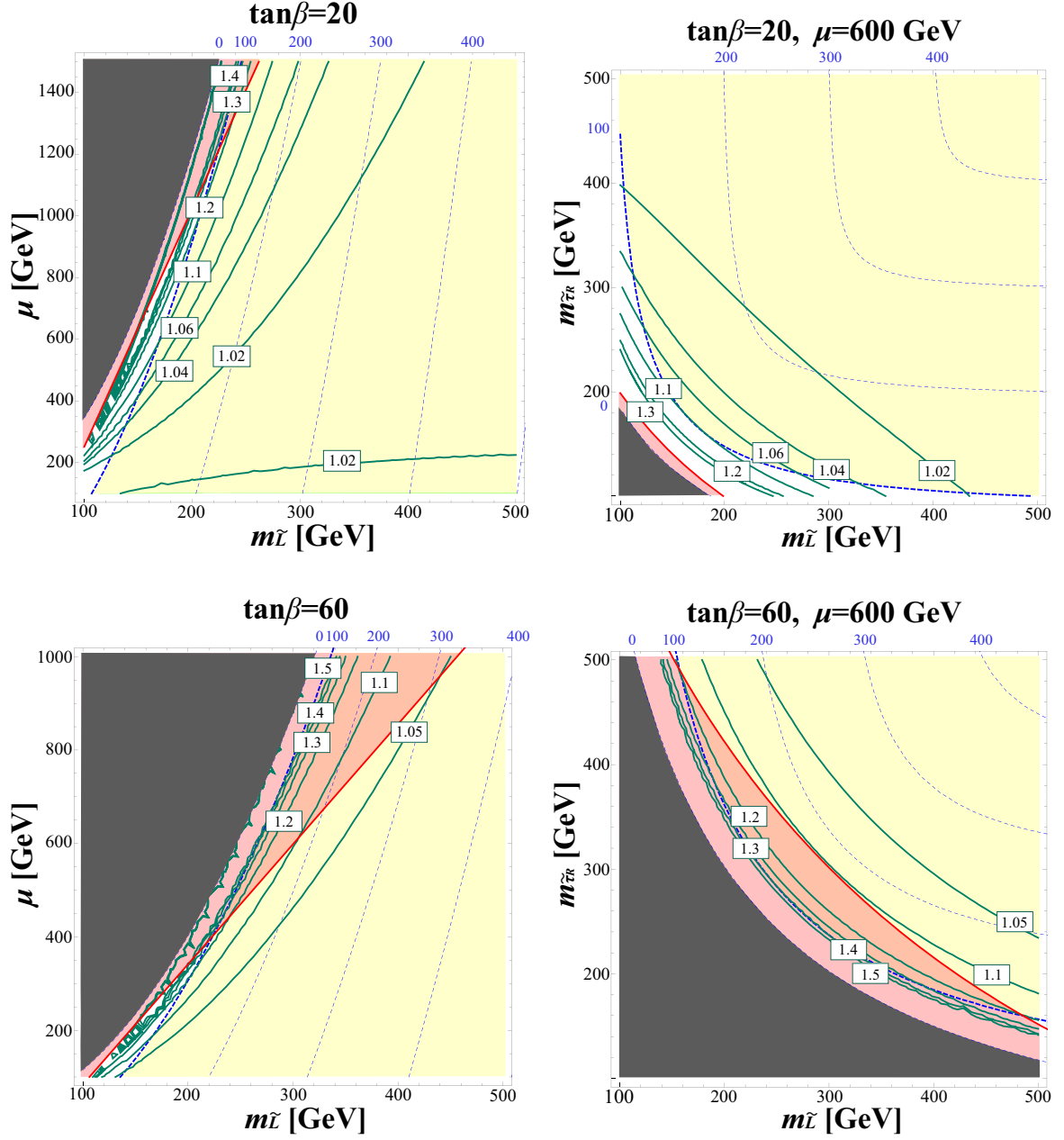


Figure 2: Solid lines are contour plots of $\Gamma(h \rightarrow \gamma\gamma)/\Gamma(h \rightarrow \gamma\gamma)_{SM}$, in the $\mu - m_{\tilde{L}}$ plane for $m_{\tilde{\tau}_R} = m_{\tilde{L}}$ (**left side**), as well as in the $m_{\tilde{L}} - m_{\tilde{\tau}_R}$ plane for $\mu = 600$ GeV (**right side**). $\tan\beta = 20$ (**top**) and $\tan\beta = 60$ (**bottom**). In all panels, $M_A = 1$ TeV, $A_\tau = 0$ GeV, $m_{\tilde{Q}_3} = m_{\tilde{t}_R} = 850$ GeV and $A_t = 1.7$ TeV giving $m_h \sim 126$ GeV at the two loop level. Dashed lines are contour plot of the lighter stau mass $m_{\tilde{\tau}_1}$. The red (gray) areas are breaking the vacuum meta-stability condition. The gray (dark gray) areas are the regions where the lighter stau is tachyonic.

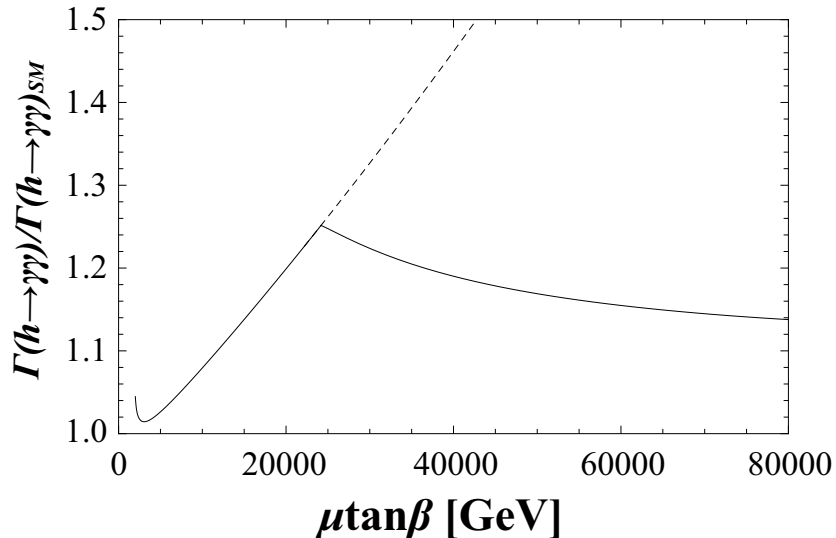


Figure 3: The upper bound line of $\Gamma(h \rightarrow \gamma\gamma)/\Gamma(h \rightarrow \gamma\gamma)_{\text{SM}}$ as a function of $\mu \tan \beta$, for $\tan \beta = 50$, varying $m_{\tilde{L}}$ and $m_{\tilde{\tau}_R}$ with remaining the lighter stau mass $m_{\tilde{\tau}_1} = 100$ GeV. Other parameters take the same value as Figure 2. If we would not consider the vacuum stability, the upper bound of $\Gamma(h \rightarrow \gamma\gamma)/\Gamma(h \rightarrow \gamma\gamma)_{\text{SM}}$ is given by the dashed line.

loop level. In our calculation, the value of $\Gamma(h \rightarrow \gamma\gamma)$ contains not only the stau loop but the full one loop order. We have checked that the results are only sensitive to $m_{\tilde{L}}$, $m_{\tilde{\tau}_R}$, μ and $\tan \beta$. On the other hand, however, we have checked that they are insensitive to the Higgs mass.

For $\tan \beta = 20$, the enhancement to $\Gamma(h \rightarrow \gamma\gamma)/\Gamma(h \rightarrow \gamma\gamma)_{\text{SM}}$ is small in the low μ region. In the high μ region, however, the enhancement becomes gradually large along light stau region. The vacuum stability condition (17) has given weak constraint to $\Gamma(h \rightarrow \gamma\gamma)/\Gamma(h \rightarrow \gamma\gamma)_{\text{SM}}$. In fact, when $\mu = 600$ GeV, there are no constraints from the vacuum stability in the $m_{\tilde{\tau}_1} \geq 100$ GeV region. Here, the case of $m_{\tilde{L}} = m_{\tilde{\tau}_R} \sim 170$ GeV gives a maximum enhancement of the diphoton rate around 10 %. On the other hand, for $\tan \beta = 60$, the enhancement of $\Gamma(h \rightarrow \gamma\gamma)/\Gamma(h \rightarrow \gamma\gamma)_{\text{SM}}$ is larger than for $\tan \beta = 20$. However, the enhancement receives more severe constraint from vacuum stability. As can be seen from the lower left and right panels of Figure 2, large enhancement areas are violating the vacuum stability. After all, for $\tan \beta = 60$, the enhancement of the diphoton rate only reaches around 20 %.

Next, we show the upper bound line of $\Gamma(h \rightarrow \gamma\gamma)/\Gamma(h \rightarrow \gamma\gamma)_{\text{SM}}$ as a function of $\mu \tan \beta$, varying $m_{\tilde{L}}$ and $m_{\tilde{\tau}_R}$ while remaining the lighter stau mass $m_{\tilde{\tau}_1} = 100$ GeV, see Figure 3. We fixed $\tan \beta = 50$, and all other parameters take the same values as Figure 2. In the low $\mu \tan \beta$ region, $\mu \tan \beta \lesssim 24$ TeV, there are no constraints from vacuum stability for $m_{\tilde{\tau}_1} \geq 100$ GeV, like these encountered in the upper right panels of Figure 2. Note that the peak at very low $\mu \tan \beta$ is caused by the light

chargino loop. On the other hand, in the high $\mu \tan \beta$ region, $24 \text{ TeV} \lesssim \mu \tan \beta$, the vacuum stability condition line and the $m_{\tilde{\tau}_1} = 100 \text{ GeV}$ line begin to cross like in the lower right panels of Figure 2. Hence, vacuum stability severely constrains $\Gamma(h \rightarrow \gamma\gamma)/\Gamma(h \rightarrow \gamma\gamma)_{\text{SM}}$. If we would not consider the vacuum stability, the upper bound line of $\Gamma(h \rightarrow \gamma\gamma)/\Gamma(h \rightarrow \gamma\gamma)_{\text{SM}}$ would be given by the dashed line. Note that although in Figure 3 we fixed $\tan \beta = 50$, we have checked that these results are in fact insensitive to $\tan \beta$, but sensitive to $\mu \tan \beta$. The reason is that the stau mass matrix, the vacuum stability condition (17) and the ratio $\Gamma(h \rightarrow \gamma\gamma)/\Gamma(h \rightarrow \gamma\gamma)_{\text{SM}}$ are dependent on the form of $\mu \tan \beta$ in the large $\mu \tan \beta$ region. Thus we found that the Higgs to diphoton decay rate can increase only by 25% compared to SM value, at $\mu \tan \beta \sim 24 \text{ TeV}$ in the MSSM.

For completeness, we probed the distribution of $\Gamma(h \rightarrow \gamma\gamma)/\Gamma(h \rightarrow \gamma\gamma)_{\text{SM}}$ by scanning the parameter space of the MSSM. Although there are many parameters in the MSSM, most of them (for example, M_2 and M_A) hardly influence the upper bound of $\Gamma(h \rightarrow \gamma\gamma)/\Gamma(h \rightarrow \gamma\gamma)_{\text{SM}}$ and we have checked this numerically. Therefore, we scanned only those parameters sensitive to $\Gamma(h \rightarrow \gamma\gamma)/\Gamma(h \rightarrow \gamma\gamma)_{\text{SM}}$ as follows,

$$\begin{aligned}
100 \text{ GeV} &\leq m_{\tilde{L}} \leq 1 \text{ TeV}, \\
100 \text{ GeV} &\leq m_{\tilde{\tau}_R} \leq 1 \text{ TeV}, \\
200 \text{ GeV} &\leq \mu \leq 1.5 \text{ TeV}, \\
20 &\leq \tan \beta \leq 60.
\end{aligned} \tag{19}$$

We considered a total of one million points, where all input parameters are value of the low energy scale. Scatter plots of the results are drawn in Figure 4. We show $\Gamma(h \rightarrow \gamma\gamma)/\Gamma(h \rightarrow \gamma\gamma)_{\text{SM}}$ as a function of $\mu \tan \beta$ (left panel), $\tan \beta$ (right panel) and the lighter stau mass $m_{\tilde{\tau}_1}$ (bottom panel) in the MSSM. The other parameters of Eq. (19) take the same values as Figure 2. The red (dark gray) circles denote the case of violating vacuum meta-stability and $m_{\tilde{\tau}_1} > 0 \text{ GeV}$. The gray circles denote the case of satisfying vacuum meta-stability and $100 \text{ GeV} > m_{\tilde{\tau}_1} > 0 \text{ GeV}$. The blue (black) circles denote the case of satisfying vacuum meta-stability and $m_{\tilde{\tau}_1} > 100 \text{ GeV}$.

In the panel plotted as a function of $\mu \tan \beta$, the upper bound line of $\Gamma(h \rightarrow \gamma\gamma)/\Gamma(h \rightarrow \gamma\gamma)_{\text{SM}}$ (the blue (black) circles) reproduced the results of Figure 3. Note that since we scanned $m_{\tilde{L}}, m_{\tilde{\tau}_R} < 1 \text{ TeV}$, the upper bound line of $\Gamma(h \rightarrow \gamma\gamma)/\Gamma(h \rightarrow \gamma\gamma)_{\text{SM}}$ could not be reproduced in the large $\mu \tan \beta$ region. In the panel plotted as a function of $\tan \beta$, we found that the upper bound of $\Gamma(h \rightarrow \gamma\gamma)/\Gamma(h \rightarrow \gamma\gamma)_{\text{SM}}$ is independent of $\tan \beta$. This implies that the upper bounds are determined only by the value of $\mu \tan \beta$. Finally, in the last panel (plotted as a function of $m_{\tilde{\tau}_1}$), we found that $\Gamma(h \rightarrow \gamma\gamma)/\Gamma(h \rightarrow \gamma\gamma)_{\text{SM}}$ is severely constrained by the vacuum stability in the light stau mass region. As a result, in the case of $m_{\tilde{\tau}_1} = 200 \text{ GeV}$, 120 GeV , 100 GeV and 80 GeV , the upper bounds of the enhancement are 9%, 20%, 25% and 40%, respectively. Without considering vacuum stability, in the case of $m_{\tilde{\tau}_1} = 100 \text{ GeV}$, the upper bound of the enhancement is as large as 100% in the scanned parameters region (19).

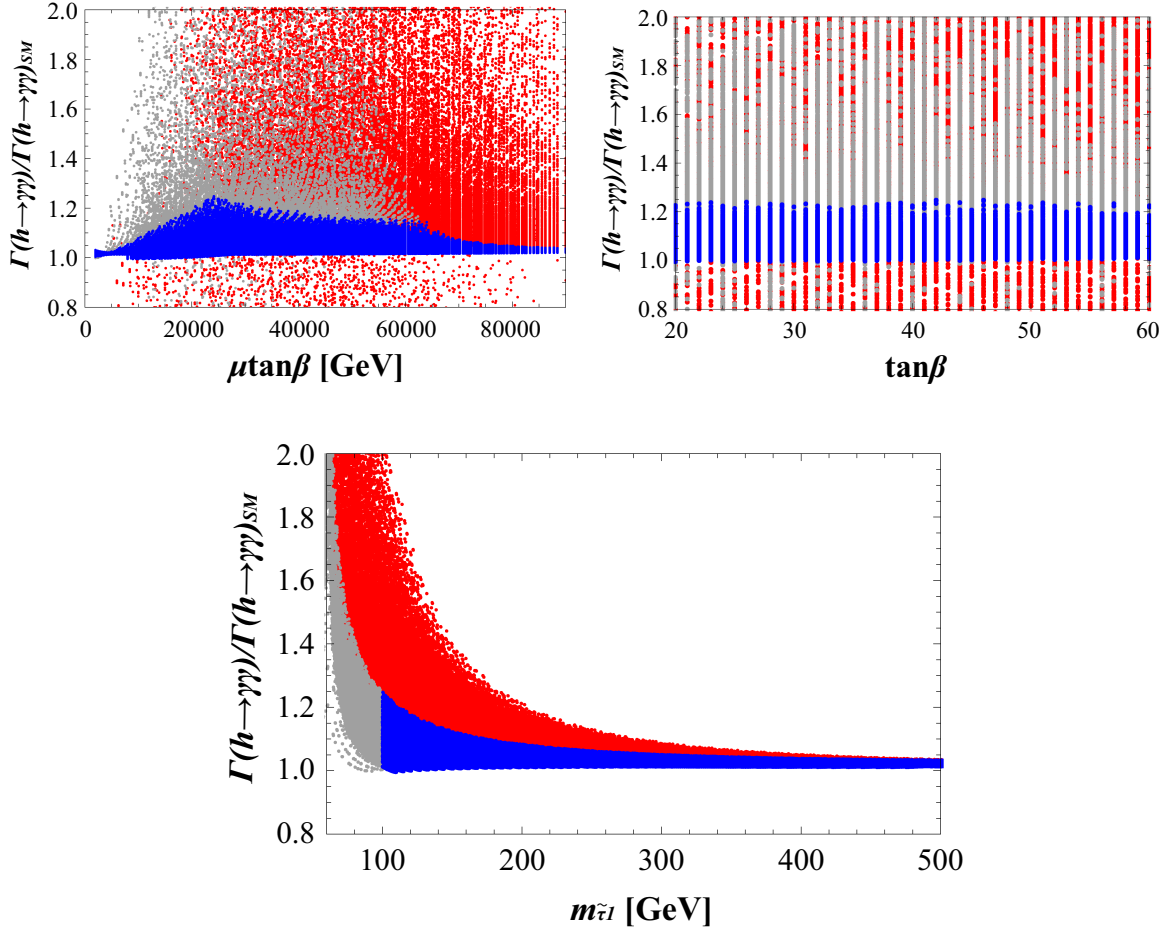


Figure 4: The scatter plots of $\Gamma(h \rightarrow \gamma\gamma)/\Gamma(h \rightarrow \gamma\gamma)_{SM}$ as a function of $\mu \tan\beta$ (**left**), $\tan\beta$ (**right**) and the lighter stau mass $m_{\tilde{\tau}_1}$ (**bottom**) in the MSSM. Parameter scan ranges are shown in Eq. (19), and other parameters take the same values as Figure 2. The red (dark gray) circles denote the case of violating vacuum meta-stability and $m_{\tilde{\tau}_1} > 0 \text{ GeV}$. The gray circles denote the case of satisfying vacuum meta-stability and $100 \text{ GeV} > m_{\tilde{\tau}_1} > 0 \text{ GeV}$. The blue (black) circles denote the case of satisfying vacuum meta-stability and $m_{\tilde{\tau}_1} > 100 \text{ GeV}$.

5 Conclusions and Discussion

In this paper, motivated by recent observations of an enhanced diphoton Higgs decay and consistent WW / ZZ Higgs decay, we first analyzed the ratio $\Gamma(h \rightarrow \gamma\gamma)/\Gamma(h \rightarrow \gamma\gamma)_{SM}$ in a broad parameter region in the MSSM while applying the stau vacuum meta-stability conditions. We found that the parameter regions of large enhancement to $\Gamma(h \rightarrow \gamma\gamma)/\Gamma(h \rightarrow \gamma\gamma)_{SM}$ are severely constrained from vacuum stability. We showed that in the case of the lighter stau mass $m_{\tilde{\tau}_1} = 200$ GeV, 120 GeV, 100 GeV and 80 GeV, the upper bounds on the enhancement to the Higgs to diphoton rate are 9%, 20%, 25% and 40%, respectively. Especially, in the case of $m_{\tilde{\tau}_1} = 100$ GeV, $\mu \tan\beta \sim 24$ TeV gives the largest enhancement to the Higgs to diphoton rate.

This result implies that if the stability of the scalar potential is taken into consideration, a large deviation between the diphoton and WW/ZZ signal strengths can not be achieved in the MSSM. Another implication is that if we require a 30% enhancement to the diphoton signal strength in the MSSM, $\sigma(pp \rightarrow h)/\sigma(pp \rightarrow h)_{SM} \times \Gamma(h \rightarrow \text{All})_{SM}/\Gamma(h \rightarrow \text{All})$ is required to be enhanced, and hence an enhancement to the WW/ZZ signal strength becomes inevitable.

Note that the vacuum stability condition used in this paper arises from the tree-level scalar potential [28]. One should take into account the vacuum stability condition which includes higher-order correction since the parameter regions which can enhance the diphoton rate would receive large higher-order corrections. However, the estimation of the vacuum stability condition which includes higher-order correction is complicated and the author reserves the study of the higher-order vacuum stability condition for future work.

Furthermore, note that not only in the MSSM but also in general models, “light charged scalar particles scenarios” or “light charged vector-like lepton scenarios” would need large cubic or large quartic interaction with the Higgs boson in order to enhance the diphoton signal strength [3, 9]. Large cubic scalar interaction, however, may suffer from vacuum instability just like the MSSM. Also, large quartic interaction may suffer from vacuum instability when dimensionless couplings become negative values, and from Landau poles when dimensionless couplings rapidly blow up at high scales. Hence in the light charged scalar particle or vector-like lepton scenarios, the consideration of the vacuum stability and Landau pole is desirable.

At the end of this project, the Ref. [42] was posted on arXiv. The authors of this paper also first applied the vacuum meta-stability to the diphoton signal strength in some gauge mediation models. As a result, they showed that the parameter regions which are consistent with the Higgs mass and muon $g - 2$ can enhance the $BR(h \rightarrow \gamma\gamma)/BR(h \rightarrow \gamma\gamma)_{SM}$ to 20% – 30%.

Acknowledgements

The author would like to thank Takeo Moroi for useful discussions, and also thank Koichi Hamaguchi and Motoi Endo for motive argument of this paper.

Appendix

A Loop functions and Higgs couplings

The Loop functions $A_i^h(\tau)$ are given as follows

$$\begin{aligned} A_1^h(\tau) &= 2 + 3\tau + 3\tau(2 - \tau)f(\tau), \\ A_{\frac{1}{2}}^h(\tau) &= -2\tau(1 + (1 - \tau)f(\tau)), \\ A_0^h(\tau) &= \tau(1 - \tau f(\tau)), \end{aligned} \quad (20)$$

and

$$f(\tau) = \begin{cases} \arcsin^2\left(\sqrt{\frac{1}{\tau}}\right), & \text{if } \tau \geq 1, \\ -\frac{1}{4} \left(\ln\left(\frac{\eta_+}{\eta_-}\right) - i\pi\right)^2, & \text{if } \tau \leq 1, \end{cases} \quad (21)$$

where

$$\eta_{\pm} \equiv (1 \pm \sqrt{1 - \tau}). \quad (22)$$

In the MSSM, the Higgs coupling constants are given as follows

$$g_{hWW} = \frac{g^2 v}{\sqrt{2}} \sin(\beta - \alpha), \quad (23)$$

$$g_{hff(\text{up type})} = \frac{m_f \cos \alpha}{\sqrt{2} v \sin \beta}, \quad (24)$$

$$g_{hff(\text{down type})} = \frac{m_f - \sin \alpha}{\sqrt{2} v \cos \beta}, \quad (25)$$

$$\begin{aligned} g_{h\tilde{f}_i\tilde{f}_i(\text{up type})} &= \left((-I_{3,L} + (I_{3,L} + Y_L) \sin^2 \theta_W) \frac{gm_Z}{\cos \theta_W} \sin(\alpha + \beta) + \frac{\sqrt{2}m_f^2 \cos \alpha}{v \sin \beta} \right) (x_L^{f_i})^2 \\ &+ \left(-Y_R \sin^2 \theta_W \frac{gm_Z}{\cos \theta_W} \sin(\alpha + \beta) + \frac{\sqrt{2}m_f^2 \cos \alpha}{v \sin \beta} \right) (x_R^{f_i})^2 \\ &+ \frac{\sqrt{2}m_f \mu \sin \alpha + A_f \cos \alpha}{v \sin \beta} x_L^{f_i} x_R^{f_i}, \end{aligned} \quad (26)$$

$$\begin{aligned} g_{h\tilde{f}_i\tilde{f}_i(\text{down type})} &= \left((-I_{3,L} + (I_{3,L} + Y_L) \sin^2 \theta_W) \frac{gm_Z}{\cos \theta_W} \sin(\alpha + \beta) - \frac{\sqrt{2}m_f^2 \sin \alpha}{v \cos \beta} \right) (x_L^{f_i})^2 \\ &+ \left(-Y_R \sin^2 \theta_W \frac{gm_Z}{\cos \theta_W} \sin(\alpha + \beta) - \frac{\sqrt{2}m_f^2 \sin \alpha}{v \cos \beta} \right) (x_R^{f_i})^2 \\ &- \frac{\sqrt{2}m_f \mu \cos \alpha + A_f \sin \alpha}{v \cos \beta} x_L^{f_i} x_R^{f_i}, \end{aligned} \quad (27)$$

$$g_{h\chi_i^+ \chi_i^-} = \frac{g}{\sqrt{2}} (-\mathbf{V}_{i1} \mathbf{U}_{i2} \sin \alpha + \mathbf{V}_{i2} \mathbf{U}_{i1} \cos \alpha), \quad (28)$$

$$g_{hH^+ H^-} = g \left(m_W \sin(\beta - \alpha) + \frac{m_Z \cos 2\beta}{2 \cos \theta_W} \sin(\alpha + \beta) \right), \quad (29)$$

where $Y_{L/R}$ and $I_{3,L/R}$ are hypercharge and isospin of left/right-handed sfermion, sfermion mass eigenstates are $\tilde{f}_i = x_L^{f_i} \tilde{f}_L + x_R^{f_i} \tilde{f}_R$, θ_W is the Weinberg angle, and α is a rotation angle which translates the gauge-eigenstate basis CP-even Higgs mass matrix into the mass-eigenstate basis. The chargino mass matrix is diagonalized to a real positive diagonal mass matrix by two 2×2 unitary matrices \mathbf{U} and \mathbf{V} as follows,

$$\mathbf{U}^* \begin{pmatrix} M_2 & \sqrt{2}m_W \sin \beta \\ \sqrt{2}m_W \cos \beta & \mu \end{pmatrix} \mathbf{V}^\dagger = \begin{pmatrix} m_{\chi_1^\pm} & 0 \\ 0 & m_{\chi_2^\pm} \end{pmatrix}. \quad (30)$$

B Analysis of the global minimum of the scalar potential

In this appendix, we analyze numerically the global minimum of the scalar potential in four-field space $(h_d, h_u, \tilde{L}, \tilde{\tau}_R)$, and probe upper bound of μ requiring that the electroweak-breaking minimum is the global minimum. Note that h_u is the same as ϕ in the main text and h_d is the down-type neutral Higgs field. The tree level scalar potential which only includes dominant top/stop loop correction in four-field space is given as follows,

$$\begin{aligned} V = & (\mu^2 + m_{H_d}^2)(H_d^0)^2 + (\mu^2 + m_{H_u}^2)(H_u^0)^2 - 2B_\mu H_d^0 H_u^0 \\ & + y_\tau^2 \left((\tilde{L}^2 + \tilde{\tau}_R^2) (H_d^0)^2 + \tilde{\tau}_R^2 \tilde{L}^2 \right) - 2y_\tau \mu \tilde{\tau}_R \tilde{L} H_u^0 + m_{\tilde{L}}^2 \tilde{L}^2 + m_{\tilde{\tau}_R}^2 \tilde{\tau}_R^2 + 2y_\tau A_\tau \tilde{\tau}_R \tilde{L} H_d^0 \\ & + \frac{g'^2}{2} \left(-\frac{1}{2}(H_d^0)^2 + \frac{1}{2}(H_u^0)^2 - \frac{1}{2}\tilde{L}^2 + \tilde{\tau}_R^2 \right)^2 + \frac{g^2}{8} \left((H_d^0)^2 - (H_u^0)^2 - \tilde{L}^2 \right)^2 \\ & + \frac{g'^2 + g^2}{8} \Delta_t (H_u^0)^4, \end{aligned} \quad (31)$$

where $H_d^0 = v_1 + h_d/\sqrt{2}$, $H_u^0 = v_2 + h_u/\sqrt{2}$ and Δ_t is given by Eq. (16). The scalar potential (31) includes only real parts of scalar bosons. When the scalar potential (31) is expanded around the electroweak-breaking vacuum and the down-type neutral Higgs field is omitted, it reproduces the scalar potential (15).

In Figure 5, we show the upper bound of μ requiring that the electroweak-breaking minimum is the global minimum as a function of $m_{H_u}^2$ for $\tan \beta = 50$ (left-hand side) and $\tan \beta = 10$ (right-hand side). In both of the panels, $m_{\tilde{L}} = m_{\tilde{\tau}_R} = 400$ GeV, $A_\tau = 0$ GeV and $\Delta_t = 1$. Green dashed lines show the meta-stability bound (17). Dotted lines are contour plots of $\sqrt{B_\mu}$. Gray areas denote the regions where electroweak symmetry breaking can not be achieved.

Moreover in Figure 6, we showed the upper bound of μ requiring that the electroweak-breaking minimum is the global minimum as a function of $\sqrt{B_\mu}$. We take $\tan \beta = 10$, $m_{\tilde{L}} = m_{\tilde{\tau}_R} = 400$ GeV, $\Delta_t = 1$ and $A_\tau = 0$ GeV (blue solid line), -500 GeV (red dashed line). Green dashed line shows the meta-stability bound (17). Gray lines are contour plots of $m_{H_u}^2$.

We found that regardless of the sign of $m_{H_u}^2$, the parameter $m_{H_u}^2$ does not affect the upper bound of μ . We also found that the low $\sqrt{B_\mu}$ and low $\tan \beta$ regions can

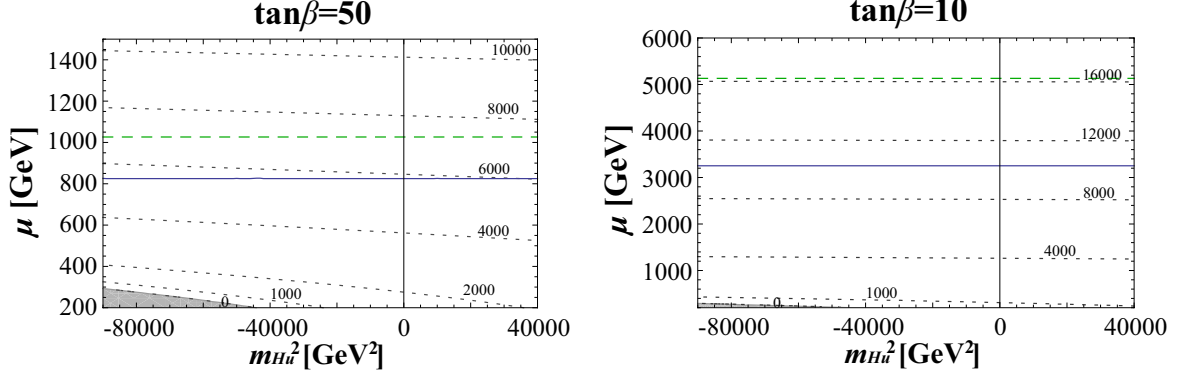


Figure 5: The upper bound of μ requiring that the electroweak-breaking minimum is the global minimum as a function of $m_{H_u}^2$. We take $\tan\beta = 50$ (**left**) and $\tan\beta = 10$ (**right**). In both of the panels, $m_{\tilde{L}} = m_{\tilde{\tau}_R} = 400$ GeV, $A_\tau = 0$ GeV and $\Delta_t = 1$. Green dashed lines show the meta-stability bound (17). Dotted lines are contour plots of $\sqrt{B_\mu}$ [GeV]. Gray areas denote the region where electroweak symmetry breaking can not be achieved.

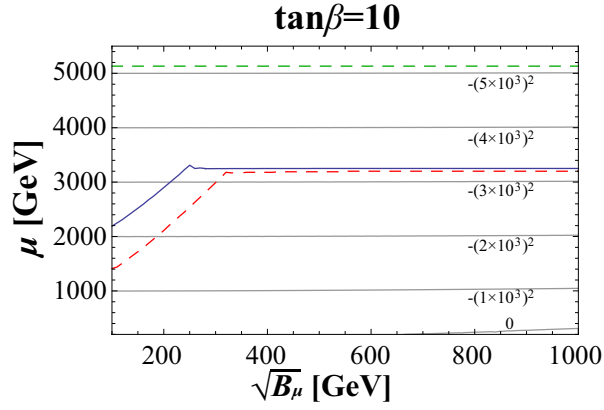


Figure 6: The upper bound of μ requiring that the electroweak-breaking minimum is the global minimum as a function of $\sqrt{B_\mu}$. We take $\tan\beta = 10$ and $A_\tau = 0$ GeV (blue solid line), -500 GeV (red dashed line). Green dashed line shows the meta-stability bound (17). Gray lines are contour plots of $m_{H_u}^2$ [GeV²].

affect the upper bound of μ and these regions are sensitive to A_τ . The reason is that because these regions exhibit low M_A , h_d component gives considerable contribution in the scalar potential (31), which then brings down another charged-breaking vacuum which becomes the global minimum earlier than the usual charged-breaking vacuum. Furthermore, we found that the shape of scalar potential (31) remains unaltered by a change of $m_{H_u}^2$ and $\sqrt{B_\mu}$, except low $\sqrt{B_\mu}$ and low $\tan\beta$ regions. These results imply that the approximate meta-stability conditional function (17) can be considered reasonable except in the low $\sqrt{B_\mu}$ and low $\tan\beta$ regions.

References

- [1] **ATLAS** Collaboration, G. Aad *et al.*, “Observation of a new particle in the search for the Standard Model Higgs boson with the ATLAS detector at the LHC,” *Phys.Lett.* **B716** (2012) 1–29, [arXiv:1207.7214 \[hep-ex\]](#).
- [2] **CMS** Collaboration, S. Chatrchyan *et al.*, “Observation of a new boson at a mass of 125 GeV with the CMS experiment at the LHC,” *Phys.Lett.* **B716** (2012) 30–61, [arXiv:1207.7235 \[hep-ex\]](#).
- [3] M. Carena, I. Low, and C. E. Wagner, “Implications of a Modified Higgs to Diphoton Decay Width,” *JHEP* **1208** (2012) 060, [arXiv:1206.1082 \[hep-ph\]](#).
- [4] C.-W. Chiang and K. Yagyu, “Higgs boson decays to $\gamma\gamma$ and $Z\gamma$ in models with Higgs extensions,” [arXiv:1207.1065 \[hep-ph\]](#).
- [5] H. Cheon and S. K. Kang, “Constraining parameter space in type-II two-Higgs doublet model in light of a 125 GeV Higgs boson,” [arXiv:1207.1083 \[hep-ph\]](#).
- [6] M. R. Buckley and D. Hooper, “Are There Hints of Light Stops in Recent Higgs Search Results?,” [arXiv:1207.1445 \[hep-ph\]](#).
- [7] H. An, T. Liu, and L.-T. Wang, “125 GeV Higgs Boson, Enhanced Di-photon Rate, and Gauged U(1)PQ-Extended MSSM,” [arXiv:1207.2473 \[hep-ph\]](#).
- [8] A. Joglekar, P. Schwaller, and C. E. Wagner, “Dark Matter and Enhanced Higgs to Di-photon Rate from Vector-like Leptons,” [arXiv:1207.4235 \[hep-ph\]](#).
- [9] N. Arkani-Hamed, K. Blum, R. T. D’Agnolo, and J. Fan, “2:1 for Naturalness at the LHC?,” [arXiv:1207.4482 \[hep-ph\]](#).
- [10] N. Haba, K. Kaneta, Y. Mimura, and R. Takahashi, “Enhancement of Higgs to diphoton decay width in non-perturbative Higgs model,” [arXiv:1207.5102 \[hep-ph\]](#).
- [11] L. G. Almeida, E. Bertuzzo, P. A. Machado, and R. Z. Funchal, “Does $H \rightarrow \gamma\gamma$ Taste like vanilla New Physics?,” [arXiv:1207.5254 \[hep-ph\]](#).

- [12] A. Delgado, G. Nardini, and M. Quiros, “Large diphoton Higgs rates from supersymmetric triplets,” [arXiv:1207.6596 \[hep-ph\]](#).
- [13] J. Kearney, A. Pierce, and N. Weiner, “Vectorlike Fermions and Higgs Couplings,” [arXiv:1207.7062 \[hep-ph\]](#).
- [14] J. R. Espinosa, C. Grojean, V. Sanz, and M. Trott, “NSUSY fits,” [arXiv:1207.7355 \[hep-ph\]](#).
- [15] I. Dorsner, S. Fajfer, A. Greljo, and J. F. Kamenik, “Higgs Uncovering Light Scalar Remnants of High Scale Matter Unification,” [arXiv:1208.1266 \[hep-ph\]](#).
- [16] K. Schmidt-Hoberg and F. Staub, “Enhanced $h \rightarrow \gamma\gamma$ rate in MSSM singlet extensions,” [arXiv:1208.1683 \[hep-ph\]](#).
- [17] M. Reece, “Vacuum Instabilities with a Wrong-Sign Higgs-Gluon-Gluon Amplitude,” [arXiv:1208.1765 \[hep-ph\]](#).
- [18] H. Davoudiasl, H.-S. Lee, and W. J. Marciano, “Dark Side of Higgs Diphoton Decays and Muon $g-2$,” [arXiv:1208.2973 \[hep-ph\]](#).
- [19] M. Carena, S. Gori, N. R. Shah, and C. E. Wagner, “A 125 GeV SM-like Higgs in the MSSM and the $\gamma\gamma$ rate,” *JHEP* **1203** (2012) 014, [arXiv:1112.3336 \[hep-ph\]](#).
- [20] J.-J. Cao, Z.-X. Heng, J. M. Yang, Y.-M. Zhang, and J.-Y. Zhu, “A SM-like Higgs near 125 GeV in low energy SUSY: a comparative study for MSSM and NMSSM,” *JHEP* **1203** (2012) 086, [arXiv:1202.5821 \[hep-ph\]](#).
- [21] M. Carena, S. Gori, N. R. Shah, C. E. Wagner, and L.-T. Wang, “Light Stau Phenomenology and the Higgs $\gamma\gamma$ Rate,” *JHEP* **1207** (2012) 175, [arXiv:1205.5842 \[hep-ph\]](#).
- [22] M. A. Ajaib, I. Gogoladze, and Q. Shafi, “Higgs Boson Production and Decay: Effects from Light Third Generation and Vectorlike Matter,” [arXiv:1207.7068 \[hep-ph\]](#).
- [23] N. D. Christensen, T. Han, and S. Su, “MSSM Higgs Bosons at The LHC,” *Phys.Rev.* **D85** (2012) 115018, [arXiv:1203.3207 \[hep-ph\]](#).
- [24] K. Hagiwara, J. S. Lee, and J. Nakamura, “Properties of 125 GeV Higgs boson in non-decoupling MSSM scenarios,” [arXiv:1207.0802 \[hep-ph\]](#).
- [25] R. Benbrik, M. G. Bock, S. Heinemeyer, O. Stal, G. Weiglein, *et al.*, “Confronting the MSSM and the NMSSM with the Discovery of a Signal in the two Photon Channel at the LHC,” [arXiv:1207.1096 \[hep-ph\]](#).

- [26] J. Casas, A. Lleyda, and C. Munoz, “Strong constraints on the parameter space of the MSSM from charge and color breaking minima,” *Nucl.Phys.* **B471** (1996) 3–58, [arXiv:hep-ph/9507294](#) [hep-ph].
- [27] R. Rattazzi and U. Sarid, “Large tan Beta in gauge mediated SUSY breaking models,” *Nucl.Phys.* **B501** (1997) 297–331, [arXiv:hep-ph/9612464](#) [hep-ph].
- [28] J. Hisano and S. Sugiyama, “Charge-breaking constraints on left-right mixing of stau’s,” *Phys.Lett.* **B696** (2011) 92–96, [arXiv:1011.0260](#) [hep-ph].
- [29] R. Dermisek and I. Low, “Probing the Stop Sector and the Sanity of the MSSM with the Higgs Boson at the LHC,” *Phys.Rev.* **D77** (2008) 035012, [arXiv:hep-ph/0701235](#) [hep-ph].
- [30] M. S. Carena, S. Heinemeyer, C. Wagner, and G. Weiglein, “Suggestions for benchmark scenarios for MSSM Higgs boson searches at hadron colliders,” *Eur.Phys.J.* **C26** (2003) 601–607, [arXiv:hep-ph/0202167](#) [hep-ph].
- [31] U. Ellwanger, “A Higgs boson near 125 GeV with enhanced di-photon signal in the NMSSM,” *JHEP* **1203** (2012) 044, [arXiv:1112.3548](#) [hep-ph].
- [32] M. A. Shifman, A. Vainshtein, M. Voloshin, and V. I. Zakharov, “Low-Energy Theorems for Higgs Boson Couplings to Photons,” *Sov.J.Nucl.Phys.* **30** (1979) 711–716.
- [33] G. K. S. D. John F. Gunion, Howard E. Haber, *The Higgs hunter’s guide*. Westview Press, 1990.
- [34] **Tevatron Electroweak Working Group, for the CDF and D0** Collaboration, M. Lancaster, “Combination of CDF and D0 results on the mass of the top quark using up to 5.8 fb⁻¹ of data,” [arXiv:1107.5255](#) [hep-ex].
- [35] M. A. Diaz and P. Fileviez Perez, “Can we distinguish between h(SM) and h0 in split supersymmetry?,” *J.Phys.G* **G31** (2005) 563–569, [arXiv:hep-ph/0412066](#) [hep-ph].
- [36] G. F. Giudice, P. Paradisi, and A. Strumia, “Correlation between the Higgs Decay Rate to Two Photons and the Muon $g - 2$,” [arXiv:1207.6393](#) [hep-ph].
- [37] K. Hagiwara, R. Liao, A. D. Martin, D. Nomura, and T. Teubner, “ $(g - 2)_\mu$ and $\alpha(M_Z^2)$ re-evaluated using new precise data,” *J.Phys.G* **G38** (2011) 085003, [arXiv:1105.3149](#) [hep-ph].
- [38] T. Moroi, “The Muon anomalous magnetic dipole moment in the minimal supersymmetric standard model,” *Phys.Rev.* **D53** (1996) 6565–6575, [arXiv:hep-ph/9512396](#) [hep-ph].
- [39] S. R. Coleman, “The Fate of the False Vacuum. 1. Semiclassical Theory,” *Phys.Rev.* **D15** (1977) 2929–2936.

- [40] C. Csaki, A. Falkowski, Y. Nomura, and T. Volansky, “New Approach to the μ -Bmu Problem of Gauge-Mediated Supersymmetry Breaking,” *Phys.Rev.Lett.* **102** (2009) 111801, [arXiv:0809.4492](#) [hep-ph].
- [41] **Particle Data Group** Collaboration, J. Beringer *et al.*, “Review of Particle Physics (RPP),” *Phys.Rev.* **D86** (2012) 010001.
- [42] R. Sato, K. Tobioka, and N. Yokozaki, “Enhanced Diphoton Signal of the Higgs Boson and the Muon $g-2$ in Gauge Mediation Models,” [arXiv:1208.2630](#) [hep-ph].